THE JOURNAL OF BIOLOGICAL CHEMISTRY VOL. 290, NO. 18, pp. 11479–11490, May 1, 2015

Fluorescence Resonance Energy Transfer (FRET) and Proximity Ligation Assays Reveal Functionally Relevant Homo- and Heteromeric Complexes among Hyaluronan Synthases HAS1, HAS2, and HAS3*

Received for publication, January 25, 2015, and in revised form, March 15, 2015 Published, JBC Papers in Press, March 20, 2015, DOI 10.1074/jbc.M115.640581

Geneviève Bart[‡], Nuria Ortega Vico[§], Antti Hassinen[§], Francois M. Pujol[§], Ashik Jawahar Deen[‡1], Aino Ruusala[¶], Raija H. Tammi[‡], Anthony Squire[‖], Paraskevi Heldin[¶], Sakari Kellokumpu[§], and Markku I. Tammi[‡2]

From the [‡]Institute of Biomedicine/Anatomy, University of Eastern Finland, FI-70211 Kuopio, Finland, the [§]Faculty of Biochemistry and Molecular Medicine, University of Oulu, FI-90014 Oulu, Finland, the [¶]Ludwig Institute for Cancer Research, Uppsala University, SE-75124, Uppsala, Sweden, and the [‖]Institute for Experimental Immunology and Imaging, University Clinic Essen, 45147 Essen, Germany

Background: Co-immunoprecipitation experiments suggest the existence of HAS2-HAS2 and HAS2-HAS3 enzyme complexes.
Results: FRET and proximity ligation assays show homo- and heteromeric complexes among all HASs.
Conclusion: Like Golgi glycosyltransferases, HASs form homo- and heteromeric complexes.
Significance: Different HAS complexes may have specific effects on hyaluronan synthesis.

In vertebrates, hyaluronan is produced in the plasma membrane from cytosolic UDP-sugar substrates by hyaluronan synthase 1–3 (HAS1–3) isoenzymes that transfer *N*-acetylglucosamine (GlcNAc) and glucuronic acid (GlcUA) in alternative positions in the growing polysaccharide chain during its simultaneous extrusion into the extracellular space. It has been shown that HAS2 immunoprecipitates contain functional HAS2 homomers and also heteromers with HAS3 (Karousou, E., Kamiryo, M., Skandalis, S. S., Ruusala, A., Asteriou, T., Passi, A., Yamashita, H., Hellman, U., Heldin, C. H., and Heldin, P. (2010) The activity of hyaluronan synthase 2 is regulated by dimerization and ubiquitination. *J. Biol. Chem.* 285, 23647–23654). Here we have systematically screened in live cells, potential interactions among the HAS isoenzymes using fluorescence resonance energy transfer (FRET) and flow cytometric quantification. We show that all HAS isoenzymes form homomeric and also heteromeric complexes with each other. The same complexes were detected both in Golgi apparatus and plasma membrane by using FRET microscopy and the acceptor photobleaching method. Proximity ligation assays with HAS antibodies confirmed the presence of HAS1-HAS2, HAS2-HAS2, and HAS2-HAS3 complexes between endogenously expressed HASs. C-terminal deletions revealed that the enzymes interact mainly via uncharacterized N-terminal 86-amino acid domain(s), but additional binding site(s) probably exist in their C-terminal parts. Of all the homomeric complexes HAS1 had the lowest and HAS3 the highest synthetic activity. Interestingly, HAS1 transfection reduced the synthesis of hyaluronan obtained by HAS2 and HAS3, suggesting functional cooperation between the isoenzymes. These data indicate a general tendency of HAS isoenzymes to form both homomeric and heteromeric complexes with potentially important functional consequences on hyaluronan synthesis.

Hyaluronan is a ubiquitous glycosaminoglycan present in the pericellular and extracellular matrix of most vertebrate tissues. It is a hydrophilic polysaccharide, which tends to form gels even at low concentrations (1). It serves as a space filler, providing elasticity for soft connective tissues, lubrication for synovial joints, transparency for the vitreous body, and extracellular diffusion routes for cellular nutrients and waste products (2). Hyaluronan can also be considered as a kind of cushion, buffering cells from physical and chemical impacts, as reflected by its rapidly increasing synthesis in inflammation and tissue injury. Hyaluronan is very abundant during embryonic development, where it is associated with cell migration and proliferation during organogenesis (3). A genetic defect in hyaluronan synthesis leads to a lethal failure in heart development (4). Recent research has also assigned a number of critical signaling functions to hyaluronan, mediated by its cell surface receptors (CD44 and RHAMM) (5–7) and common growth factor receptors like those of the ErbB (8), PDGF (9), and TGFβ families (10). There is now considerable interest in the metabolism of hyaluronan as a potential target of therapy in pathological processes such as cancer (11), arterial disease (12), diabetes (13), and various forms of inflammation (14).

* This work was supported by grants from the Academy of Finland (to S. K. and M. I. T.), the Sigrid Juselius Foundation (to M. I. T. and R. H. T.), the National Glycoscience Graduate School (to A. J. D., S. K., and M. I. T.), the Kuopio University Hospital (EVO/VTR funds) (to M. I. T.), the University of Eastern Finland Spearhead Funds (Cancer Center of Eastern Finland) (to M. I. T. and R. H. T.), the Magnus Ehrnrooth Foundation and the Finnish Cultural Foundation (to A. H.), and the Ludwig Institute for Cancer Research and the Swedish Cancer Society (to P. H.).
[1] Recipient of grants from the Northern Savo Cultural Foundation, the Northern Savo Cancer Funds, and Centre for International Mobility.
[2] To whom correspondence should be addressed: Inst. of Biomedicine, School of Medicine, University of Eastern Finland, Yliopistonranta 1E, P. O. Box 1627, 70211 Kuopio, Finland. Tel.: 358-40-7674826; Fax: 358-17-163032; E-mail: tammi@uef.fi.

Hyaluronan is produced by hyaluronan synthases (HAS1–3[3] in mammals). These enzymes have two different glycosyltransferase activities in a single polypeptide. Using cytosolic UDP-glucuronic acid and UDP-*N*-acetylglucosamine as donor substrates (15), they catalyze the transfer of *N*-acetylglucosamine to glucuronic acid in β1–4 linkage and glucuronic acid in β1–3 linkage to *N*-acetylglucosamine. This results in alternating positions of these monosaccharides and the formation of a repeated disaccharide structure (-GlcNAc-GlcUA-) in a linear glycosaminoglycan chain, usually of a molecular mass in the range of 10^6 to 10^7 Da (16). Unlike other vertebrate glycoconjugates, hyaluronan is not known to be built on any protein or lipid core. For *Streptococcus equisimilis* hyaluronan synthase (seHAS) the possibility of lipid or protein carriers that could initiate hyaluronan synthesis, has been excluded (17). Moreover, while HAS polypeptides are co-translationally inserted in the ER membrane and transported to the Golgi apparatus, they become activated only after reaching the plasma membrane (18). The mechanisms that turn on hyaluronan synthesis at the plasma membrane, but prevent the premature activation in intracellular membranes, remain obscure. However, substrate supply and HAS localization are dynamically coupled as depletion of UDP-GlcUA (19) or UDP-GlcNAc (20) reduces the amount of HAS in the plasma membrane. Translocation of HAS between the plasma membrane and intracellular membranes involves vesicular trafficking factors like Rab10 (21).

Active hyaluronan synthesis at plasma membrane also requires a pore for simultaneous extrusion of the growing polysaccharide chain into the extracellular space. Streptococcal HAS itself forms the pore together with phospholipids, (17, 22), although this has not been firmly demonstrated for vertebrate HASs. Modulation of multidrug-resistant transporter activity affects hyaluronan synthesis in mammalian cells, and multidrug resistant proteins have been suggested to mediate hyaluronan transport (23). However, the evidence of hyaluronan extrusion through separate transporters has remained circumstantial, and their role has been disputed (24). The fact that hyaluronan is not generally detected in the cytosolic side of the plasma membrane (25), where it should be found if entering a separate extrusion channel, speaks against the existence of a separate pore for hyaluronan export. This is also consistent with the findings that streptococcal (26) and *Xenopus* XlHAS1 (27) are active without interaction with other proteins.

Bacterial exopolysaccharide synthesis also involves membrane-associated glycosyltransferases that presumably form a translocation pore for the transfer of their product into the periplasm. For example, the extrusion pore of the poly-β-1,6-*N*-acetylglucosamine synthesis machinery of *Yersinia pestis* (28) and *Escherichia coli* (29) is suggested to require the formation of a heterodimer with altogether 6 transmembrane domains. On the other hand, channels such as lactose permease contain 12 transmembrane α-helices (30), whereas the two protein subunits of bacterial cellulose synthase contain altogether 9 transmembrane domains and couple polymerization with membrane penetration (31). The closest relatives of the HASs, the insect chitin synthases, contain up to 16 membrane-spanning α-helices and are likely functional as dimers or oligomers (32).

For HAS enzymes, the previously proposed schematic structures (15) have not considered the possibility of homo- or heteromeric HAS complexes. Indeed, this possibility was raised for the first time in a recent study in which co-immunoprecipitation experiments demonstrated that HAS2 forms homomeric complexes and even heteromeric complexes with HAS3 (33). The functional importance of the homomeric interactions of HAS2 was demonstrated when an enzymatically inactive HAS2 mutant showed a dominant negative effect on hyaluronan synthesis when co-transfected with an enzymatically active HAS2 (33). In the present work, we have explored potential homo- and heteromeric interactions among mammalian HAS isoforms in cells *in situ* using fluorescence resonance energy transfer (FRET) and proximity ligation assays (PLA). The results establish that all three human HAS isoforms can interact with each other. The data also suggest that the different HAS isoenzyme combinations expressed in various cells and cellular environments may have specific effects on hyaluronan biosynthesis.

EXPERIMENTAL PROCEDURES

Plasmid Constructs for Flow Cytometry—The plasmids for flow cytometric FRET analyses were made as follows. The functional open reading frames (ORF) of human hyaluronan synthase genes, *Has1* (NCBI nucleotide accession number NM_001523), *Has2* (NM_005328), and *Has3* (NM_005329) were amplified from human cDNA and first ligated in-frame with the pDendra2-C vector (Evrogen, Moscow). The HAS cDNAs in Dendra2 plasmids were subcloned by 25 cycles of PCR with *pfu* polymerase (Fermentas) into either the pcDNA3-Myc tag vector (HAS1 and HAS3) or the pcDNA3-HA tag vector (HAS2) using the HindIII and XhoI restriction sites and the following primers: 5′-HAS1, ATTAAAGCTTATGAGACAGCAGGACGCGC, and 3′-HAS1, ATTACTCGAGCACCTGGACGCGGTAGC; 5′-HAS2, ATTAAAGCTTATGCATTGTGAGAGGTTTCTATGTATC, and 3′-HAS2, ATTACTCGAGTACATCAAGCACCATGTCATATTGT; and 5′-HAS3, ATTAAAGCTTATGCCGGTGCAGCTG, and 3′-HAS3, ATTACTCGAGCACCTCAGCAAAAGCCAAG.

All of the constructs were sequenced to verify that no mutations had arisen. Primers for pcDNA3 forward and reverse (Fwd, ACGACTCACTATAGGGAGAC; Rev, AATGCTAGAGCTCGCTGATC) were used for the sequencing together with new ones (designed to sequence from about 500 bp inside each gene (HAS1, GGGAGGTGGAGGCG; HAS2, TGCAAAAATGGGGTGG; and HAS3, CGTGCATCATGCAGAAGT) to allow complete sequencing of the constructs. Each HAS cDNA was PCR-amplified, and the product was inserted into the pcDNA3 vector (Clontech) using HindIII and XhoI restriction sites and the sequences verified. The vector also contained sequences encoding a C-terminal 5-amino acid linker region (RSIAT) followed by either the monomeric Cerulean (mCer),

[3] The abbreviations used are: HAS, hyaluronan synthase; HA, hyaluronic acid; PLA, proximity ligation assay; EGFP, enhanced green fluorescent protein; EYFP, enhanced yellow fluorescent protein; RFP, red fluorescent protein; mCer, monomeric Cerulean (cyan fluorescent protein); mVen, monomeric Venus (yellow fluorescent protein); mCherry, monomeric Cherry (red fluorescent protein); ER, endoplasmic reticulum.

monomeric Venus (mVen), HA (YPYDVPDYA), or Myc (EQKLISEEDL) tag (34). Thus, the constructs for flow cytometric FRET had the tags in the C terminus of the HASs.

Plasmids for the Microscopic FRET Analyses and Co-immunoprecipitations—EGFP-HAS1 was created by inserting the XhoI-EcoRI fragment from the Dendra2-HAS1 plasmid into the pEGFP-C1 vector. mCherry-HAS1 was created by ligating together mCherry with NheI-BglII, HAS1 BglII-EcoRI, and pCI-Neo NheI-EcoRI. mCherry-Has2 was created by ligating together mCherry NheI-BglII, HAS2 BglII-SalI, and pCI-Neo NheI-SalI. The construction of EGFP-HAS2, EGFP-HAS3, and mRFP-HAS3 have been described elsewhere (21). mCherry-HAS3 was created by ligating together mCherry NheI-XhoI, HAS3 XhoI-EcoRI, and pCI-Neo with XhoI-EcoRI. C-terminally truncated EGFP-HAS1 (143 residues) was created by the digestion of EGFP-HAS1 with SalI followed by religation. C-terminally truncated mCherry-HAS3 (220 residues) and EGFP-HAS3 (166 residues) were made by digestion with BamHI and PstI, respectively, before religation. C-terminally truncated EGFP-HAS3–86 was produced by digesting EGFP-HAS3 (86 residues) with SacII and religation. N-terminally truncated HAS3 was produced by ligating together the HAS3 C-terminal fragments SacII-EcoRI, EGFP-C3 NheI-SacII, and PCIneo NheI-EcoRI. C-terminally mCherry-tagged HAS3 was created by replacing Cerulean with mCherry in pcDNA3-HAS3-Cer in XhoI-NotI restriction sites.

Co-immunoprecipitation—COS1 cells were co-transfected with EGFP-HAS1, -2, or -3 and mCherry-HAS1 or -2 or mRFP-HAS3 in a 1:1 ratio. The efficiency of transfection and the presence of both fluorophores in cells were verified by microscopy. 24–30 h after transfection the cells were scraped from the plates, and membrane proteins were prepared as described elsewhere (33), immunoprecipitated using RFP-trap-M (ChromoTek GmbH, Munich, Germany), and eluted from the beads in an SDS-PAGE sample buffer (0.125 M Tris-HCl, pH 6.8, with 4% SDS, 20% glycerol, 0.2 M ditiothreitol, and 0.02% bromphenol blue) for 15 min at 65 °C. Co-precipitation was tested in Western blots with anti-GFP antibody (Invitrogen) and imaged with an Odyssey infrared system (LI-COR, Lincoln, NE).

Immunofluorescence Microscopy and FRET Flow Cytometry—COS7, COS1, HeLa, and MCF7 cells were cultivated in DMEM as described elsewhere (34, 35). One day after plating, the cells were transfected using 0.5 μg of each plasmid cDNA and the FuGENE 6^{TM} transfection reagent (Roche Applied Science). After cultivation for 24 h at 37 or 30 °C, the cells were used for fluorescence microscopy, flow cytometric FRET, or enzyme activity measurements (hyaluronan synthesis).

Cells were processed for indirect immunofluorescence as described previously (36). After fixation, the cells were permeabilized with 1 ml of 0.1% saponin in 1% BSA-PBS, pH 7.4, and stained with the Golgi marker antibody (anti-GM130 610822, BD Biosciences) and Alexa Fluor 594-conjugated secondary antibodies (Invitrogen). After staining, the cells were imaged using a Zeiss Observer Z1 equipped with a LSM 700 confocal unit, 63 × PlanApo oil immersion objective, the appropriate filter sets for CFP, YFP, and Alexa Fluor 594, and ZEN 2009 software (Carl Zeiss AG, Oberkochen, Germany).

FRET measurements were done as described (35). Briefly, 1 day after plating, the cells were transfected with the FRET plasmid constructs that encoded selected enzymes tagged with either mCer or mVen. After 24 h, the cells were detached from the plates with 2× trypsin-EDTA (Sigma-Aldrich), diluted, and analyzed on a flow cytometer (CyFlow, Partec GmbH, Münster, Germany) equipped with the appropriate filter sets for mCer (405 ex and 425–475 em) and mVen (488 ex, 515–540 em). In each measurement, 2–5 × 10^3 cells expressing both mCer and mVen were selected by gating (for setting and validation of the gates, see Ref. 34) and quantified in triplicate from three different experiments (as mCer/mVen ratios). The FRET filter set (405 ex and 515–540 em) and FloMax software were used for quantification. The FRET signal is presented as the percentage of FRET positive (FRET+) cells of those that express both the mCer and mVen constructs (mean ± S.D.). A value higher than 5% was considered relevant.

FRET Microscopy—COS1 cells were routinely cultivated in DMEM, high glucose (Invitrogen), 10% FBS (HyClone), 2 mM glutamine, and 50 units/ml penicillin (EuroClone). For experiments, cells were plated on 8-well Ibidi® chamber slides for 24 h before transfection at 15,000 cells/well. The medium level was adjusted to 200 μl just prior to transfection. Per well, 12.5 μl of 150 mM NaCl, 0.1 μg of DNA (EGFP/mCherry plasmid ratio, 1/1), and 0.5 μl of Exgen 500 Fermentas, Helsinki, Finland) were mixed. The cells were fixed 48 h after transfection in 4% paraformaldehyde for 10 min and then washed for 5 min in 50 mM Tris and 100 mM NaCl, pH 8.0, and kept in PBS at 4 °C before analysis. A Zeiss LSM700 confocal microscope with a Plan-Apochromat 40×/1.3 oil DIC M27 objective was used. Cells expressing both EGFP- and mCherry-tagged HAS constructs were examined. Images from EGFP (ex 488 nm and em 555 nm with a short pass filter) and mCherry (ex 555 nm) were taken separately. To measure FRET efficiency, mCherry was photobleached using a 555-nm laser at the maximum setting for 10–30 s, and then second pictures of both fluorophores were taken. Images were analyzed using an image-processing software package (Fiji) with ImageJ and several other plugins organized into a coherent menu structure. FRET efficiency (E) was calculated for each pixel in the bleached area as follows: $E = (I^{\text{donor post-bleach}} - I^{\text{donor pre-bleach}})/I^{\text{donor post-bleach}} \times 100$, where I^{donor} is the intensity of EGFP fluorescence. The microscopic FRET setup was essentially as described previously (37).

Proximity Ligation Assay—Normal human mesothelial cells (AG07086B, NIA, National Institutes of Health, Aging Cell Repository, Coriell Institute, Camden, NJ) were cultured in Ham's F12 medium (Sigma) supplemented with 15% FBS, 10 ng/ml human EGF (PeproTech), 0.05 μg/ml hydrocortisone (Sigma), 2 mM L-glutamine, and 1% penicillin/streptomycin (Sigma). 20,000 cells were seeded/well using 8-well chamber slides (Thermo Scientific Nunc^{TM} Lab-Tek^{TM}) and grown for 3 days. The cells were washed with PBS, fixed in 3% paraformaldehyde for 10 min, permeabilized in 0.25% Triton X-100 for 5 min, washed with PBS, blocked with 100 mM glycine, and washed again with PBS. In *situ* PLA was performed at the SciLifeLab PLA proteomics facility, Uppsala, Sweden, according to the instructions of the probe manufacturer (Olink Bioscience, Uppsala, Sweden). The cellular background for PLA was visu-

alized by incubation with 0.25 μg/ml FITC-phalloidin (Sigma) and 4′,6-diamidino-2-phenylindole (DAPI). After staining, the cells were examined with a Zeiss AxioPlan2 microscope. For counting the fluorescent dot signals, CellProfiler (Broad Institute) cell image analysis software was used. The specificity of the signal was controlled by counting the dots produced when one of the primary antibodies was omitted or replaced by preimmune serum.

The following primary antibodies at a dilution of 1 μg/ml were used for the PLA: rabbit anti-HAS1 antiserum (affinity-purified) and preimmune serum (37), HAS2 goat polyclonal antibody (sc-34067, Santa Cruz Biotechnology), rabbit anti-HAS2 antiserum (affinity-purified) and preimmune serum (38), and rabbit anti-HAS3 antiserum (Abcam 322231).

Hyaluronan Synthesis by the HAS Complexes—COS7 cells were transfected with the appropriate HAS-mCer and HAS-mVen constructs and cultivated for 24 h before the collection of growth media from the plates. The media were stored frozen at −20 °C until the hyaluronan assay (see below). The cells were washed and detached from the plates using trypsin-EDTA and analyzed by flow cytometry to determine in each plate the transfection efficiency of HAS-mCer- and -mVen constructs, the mean intensity of the fluorescent tags (a measure of the amount of each enzyme protein present), and the percentage of FRET positive cells per plate. These values were then used to normalize the original raw data values (μg of hyaluronan/ml of medium) into the corrected values. These were in turn used to calculate the activities of the various complexes relative to that of the HAS1 homomer (set at a value of 1). All cell measurements were done using three independent plates.

Tet-inducible C8161 EYFP-HAS2 melanoma cells were produced by lentiviral transduction as described elsewhere (38). The lentiviral vector was made as follows. The HAS2 coding sequence was isolated from EGFP-HAS2 plasmid cut with XhoI and EcoRI and EYFP fragment was obtained from EYFP-C1 plasmid by cutting with XhoI and Nco1, and ligated with entry vector penTTGmirc2 cut with Nco1-EcoRI. The plasmid containing all fragments in-frame was recombined into pSLICK-hygromycin (39). The cells were grown in high glucose DMEM, 10% FBS (Hyclone, Logan, UT), 2 mM L-glutamine (EuroClone), 50 μg/ml streptomycin sulfate, 50 units/ml penicillin, and 50 μg/ml hygromycin. The cells were characterized for HA secretion with different doses of doxycycline (0, 0.1, 0.25, 0.5, 1, and 2 μg/ml). 5000 C8161-EYFP-HAS2 cells were plated in a 96-well plate. After 24 h, the medium with 1% FBS was changed followed by transient transfection with 50 ng/well of HAS1-mCer, HAS3-mCer, HAS3-mVen, or empty mCer (mock) plasmids with TurboFect transfection reagent (Thermo Scientific), resulting in 50–60% transfection efficiency. 16 h later, the cells were treated with 0.25 μg/ml doxycycline. 24 h later, fluorescence (mCer, mVen, and EYFP) from the cells in each group was measured, and the media were analyzed for hyaluronan secretion with an enzyme-linked immunosorbent assay as described below.

The amount of hyaluronan secreted into the medium was determined using a sandwich-type enzyme-linked immunosorbent assay based on the hyaluronan-binding complex (containing the aggrecan G1 domain and a link protein) extracted and purified from calf articular cartilage in our laboratory (40). Briefly, MaxiSorp 96-well plates were coated with 1 μg/ml hyaluronan-binding complex, blocked with 1% bovine serum albumin in PBS, incubated with samples and hyaluronan standards, washed, and incubated with 2 μg/ml biotinylated hyaluronan-binding complex followed by the streptavidin peroxidase reaction visualized by 3,3′,5,5′-tetramethylbenzidine (41).

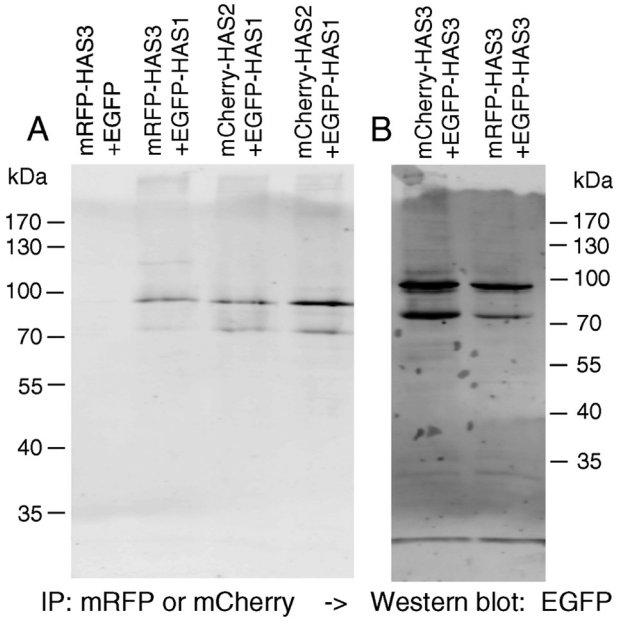

FIGURE 1. **Co-immunoprecipitations of HAS isoforms.** *A*, HAS1 co-immunoprecipitations with HAS1, HAS2, and HAS3. Beads that bind mRFP and mCherry were used to immunoprecipitate (*IP*) mRFP-HAS3, mCherry-HAS2, and mCherry-HAS1 from COS1 cultures co-transfected with EGFP-HAS1. *B*, HAS3-HAS3 co-immunoprecipitations. COS1 cells were transfected with either mCherryHAS3 and EGFP-HAS3 or mRFP-HAS3 and EGFP-HAS3 and immunoprecipitated as described in *A*. The presence of co-transfected EGFP-HAS1 (*A*) and EGFP-HAS3 (*B*) in the precipitates was analyzed by Western blotting using an anti-GFP-antibody. An EGFP plasmid without insert was used as a negative control (see *left lane* in *A*). The calculated molecular masses of EGFP-HAS1, EGFP-HAS2, and EGFP3 are 92, 90, and 90 kDa, respectively.

Statistical Analysis—Student's *t* test and one-way analysis of variance followed by Dunnett's multiple comparison test were done with GraphPad Prism5 for Windows (GraphPad Software, La Jolla, CA). Differences were considered significant if $p < 0.05$.

RESULTS

Co-immunoprecipitation of the HAS Enzyme Complexes—Mouse HAS2 enzyme was shown to form homomeric complexes by coimmunoprecipitation of FLAG- and 6myc-labeled HAS2 co-transfected in COS1 cells. Co-immunoprecipitation was also shown to take place when HAS2 and HAS3 were co-transfected, suggesting the possibility of additional heteromeric HAS complexes (33). In this study we used co-immunoprecipitations to check whether HAS1, like HAS2 and HAS3, could also form homo- and heteromeric complexes. We co-transfected EGFP-, RFP-, and mCherry-tagged HASs. Using beads that specifically bind red fluorescent proteins (including mRFP and mCherry) but not EGFP, we found that EGFP-HAS1 at the expected molecular mass of ~90 kDa was brought down by mCherry-HAS1, indicating the presence of homomeric HAS1 complexes (Fig. 1*A*). In addition, the existence of HAS1 hetero-

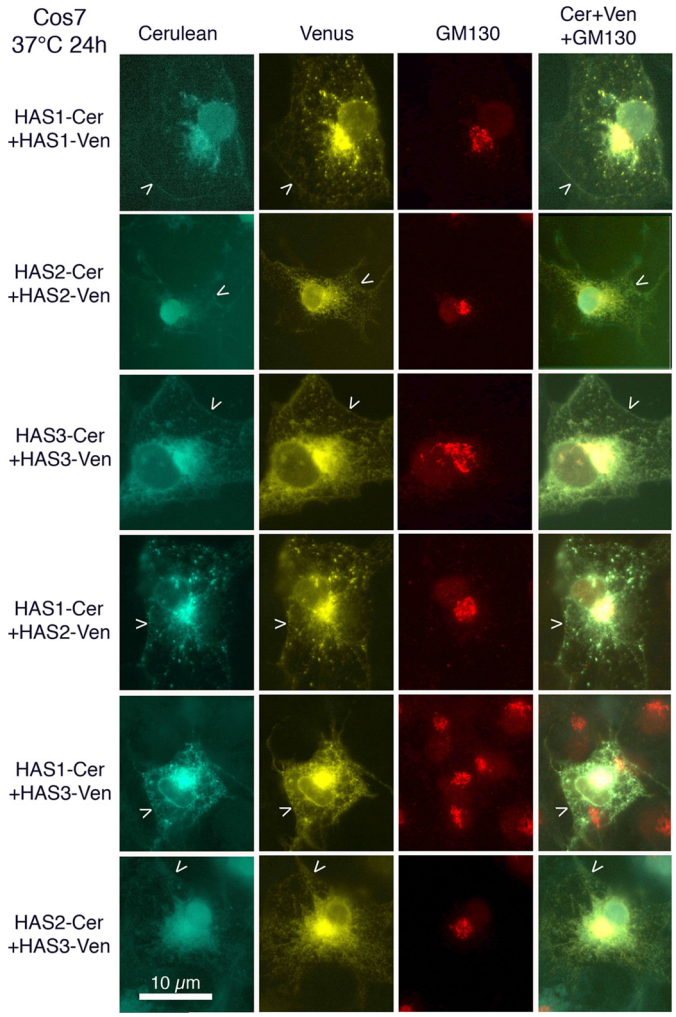

FIGURE 2. **Subcellular distribution and co-localization of HAS1, HAS2, and HAS3 with C-terminal mVen and mCer tags.** COS7 cells were transfected with the indicated constructs, fixed 24 h later, and stained with an antibody against the Golgi marker, GM130 (*red*). *Arrowheads* point to the cell surface.

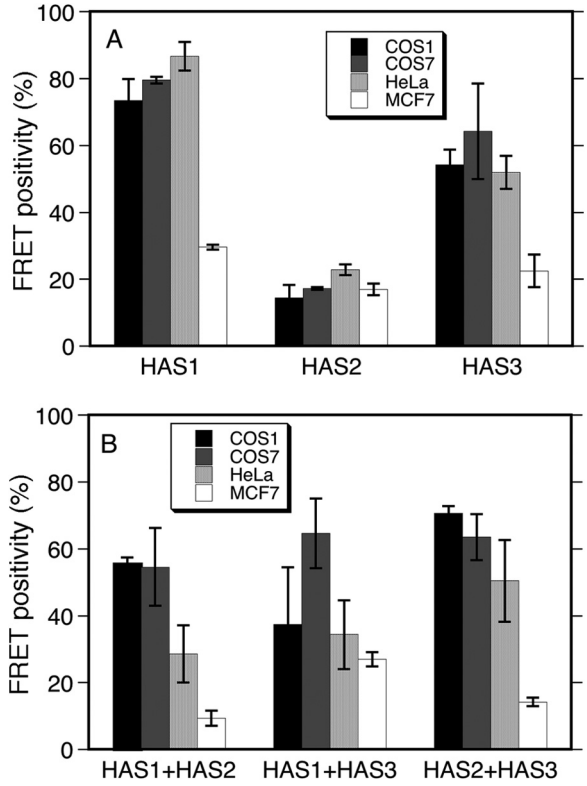

FIGURE 3. **Quantitation of the FRET signals by flow cytometry with mVen and mCer constructs in COS1, COS7, HeLa, and MCF7 cells.** The cells expressing both mVen and mCer were analyzed by flow cytometry for FRET positive cells (% of counted) in triplicate, counting 100–300 cells in each measurement. Homomeric complexes are shown in *A* and heteromeric complexes in *B*. Means ± S.D. are shown.

meric complexes with either HAS2 or HAS3 were also shown by co-immunoprecipitation with mRFP-HAS3 and mCherry-HAS2 (Fig. 1). EGFP alone was not co-immunoprecipitated with mRFP-HAS3 or mCherry-HAS2, indicating that the fluorescent tags were not responsible for complex formation. A lighter band at 70–80 kDa was also present in the immunoprecipitates, perhaps representing an EGFP-HAS1 that had lost a fragment from its C terminus but was still able to bind all HAS isoforms. HAS3 tagged with mCherry and RFP also precipitated with EGFP-HAS3, suggesting HAS3 homomerization. An earlier study (33) and the present one thus suggest that all HAS protein can be precipitated in both homo- and heteromeric complexes.

Flow Cytometric Quantification of FRET in the HAS Complexes—Immunoprecipitations require lysis and dissolution of the cells, which can potentially disrupt and change the protein associations and thus also their interactions. Additional experiments using alternative approaches were therefore done to study the presence of the complexes *in situ*, without cell disruption, utilizing FRET.

We and others have shown previously that mammalian HAS polypeptides with either N-terminal (19, 20, 42) or C-terminal (27, 43) fluorescent tags retain full enzymatic activity and are mainly detectable in the ER-Golgi area but also in the plasma membrane. Immunofluorescence microscopy revealed that our new C-terminally tagged HAS enzymes were localized predominantly in the Golgi apparatus and plasma membrane (Fig. 2), consistent with previous reports (19, 43).

Quantitation of the potential interactions among the different HAS isoenzymes with FRET-flow cytometry revealed both enzyme homomers and heteromers in all of the cell lines studied, most of them expressing relatively low levels of endogenous HAS enzymes and thus also low hyaluronan synthesis. About 60–80% of the cells expressing HAS1 or HAS3 were FRET positive, indicating the formation of enzyme homomers (Fig. 3*A*). In contrast, the amount of HAS2 homomers was markedly lower, ranging between 10 and 20% of the cells. All HAS isoenzymes also formed heteromeric complexes with each other, even though some variation was detected between the different cell types (Fig. 3*B*). In MCF7 cancer cells, the amount of both homomeric and heteromeric complexes was the lowest of the cell types tested.

The specificity of the interactions was confirmed by co-transfecting cells with non-fluorescent HAS proteins to compete with each of the FRET pairs. HAS1-Myc plasmid transfected together with the HAS1-mCer/HAS1-mVen pair reduced the FRET signal to less than 30% of the original, indi-

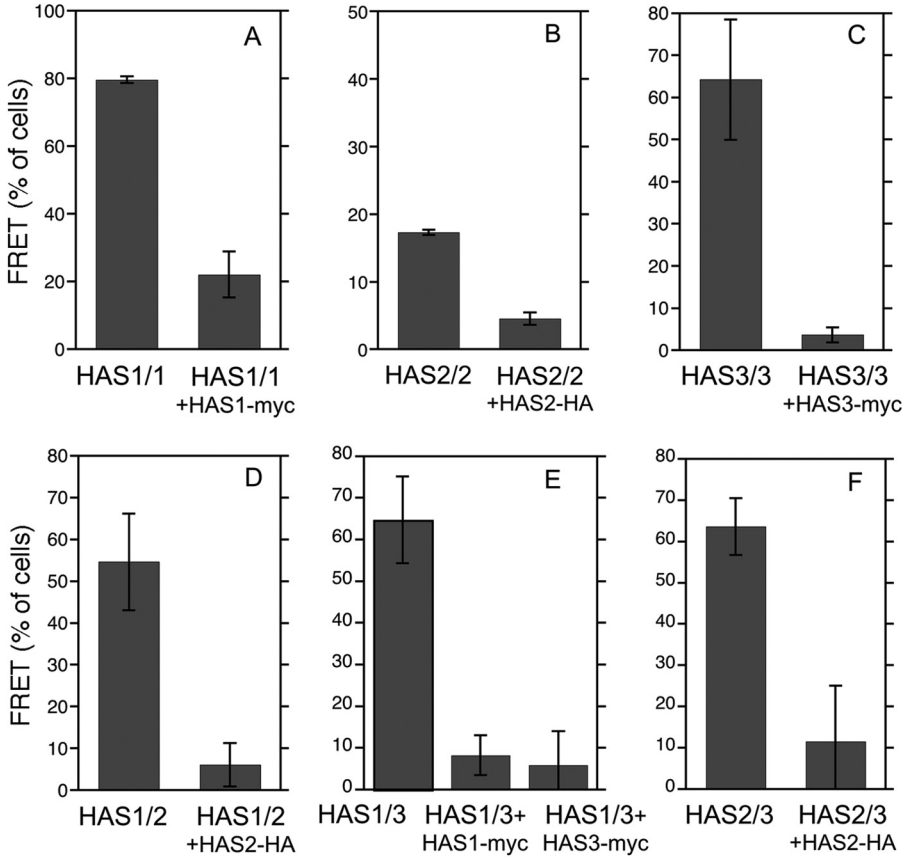

FIGURE 4. **Inhibition of FRET signal by FRET-incompatible HAS constructs.** The *left column* in each *panel* (*A–F*) shows the FRET % of the indicated HAS pair in COS7 cells. The *right columns* indicate the corresponding FRET % (mean ± S.D., $n = 3$) in the presence of competing HAS-Myc or HAS-HA constructs.

cating that the interactions are mediated by the HAS1 enzyme itself and not by the fluorescent tags (Fig. 4*A*). A similar reduction took place when HAS2 or HAS3 homomers were challenged with either HA- or Myc-tagged constructs (Fig. 4, *B* and *C*).

Similar experiments with the different HAS heteromers showed that the FRET signal of each of the complexes was markedly reduced upon co-transfection of the competing Myc- or HA-tagged enzyme construct. In all cases, heteromeric interactions were reduced to 10–30% of the original FRET signal (Fig. 4, *D–F*). Collectively, the data show that the homomeric and heteromeric interactions detected among the different HAS isoenzymes are specific and not mediated by random collisional binding events.

FRET Microscopy—The HAS proteins are known to be co-translationally inserted into the ER membrane after which they are transported through the Golgi apparatus to the plasma membrane, where they become enzymatically active (19, 43). Thus, ectopic expression of the GFP-HAS constructs results in their localization in these compartments as well as in endocytic vesicles (Fig. 2) (19, 20, 42, 43). Immunocytochemical detection of endogenously expressed HASs indicates a similar localization pattern (44). The highest amount of HAS polypeptides is generally found in the Golgi apparatus (Fig. 2).

Potential interactions among the different HAS isoenzymes and their location were studied also by FRET microscopy, using N-terminally tagged EGFP and mCherry HAS pairs, and the acceptor photobleaching method. In line with the flow cytometric analyses, significant homo- and heteromeric interactions were detected among all HAS isoenzymes. Heteromeric interactions between HAS1/HAS2, HAS1/HAS3, and HAS2/HAS3 are shown in Fig. 5*A*. These examples demonstrate the measurement polygons placed in the Golgi region where FRET was quantitated by the increase of donor fluorescence after acceptor photobleaching. Although plasma membrane contained relatively lower HAS fluorescence, FRET signal was detected there also (Fig. 5*A*, *bottom right*). The calculated FRET efficiencies for all of the homo- and heteromeric complexes are presented in Fig. 5*B*. The FRET efficiencies were relatively high, as indicated also by the low background when EGFP-HAS1 was co-transfected with mCherry alone (Fig. 5*B*).

Endogenous HAS Enzyme Complexes—To confirm that the endogenous, non-transfected HAS proteins also interact *in situ*, PLAs were used on mesothelial cells known to express all HAS isoforms. The cells were fixed and labeled with primary antibodies raised in different species, allowing distinct DNA tags in the secondary antibodies. When close enough (<40 nm), the DNA tags facilitate ligation, amplification, and a fluorescent signal. Microscopic counting of the fluorescent dots formed in the presence of goat and rabbit HAS2 antibodies revealed numerous endogenous HAS2 homomers in the cells (Fig. 6). The combination of goat HAS2 and rabbit HAS1 or HAS3 antibodies also revealed the presence of endogenous heteromeric complexes between HAS1 and HAS2 and between HAS2 and

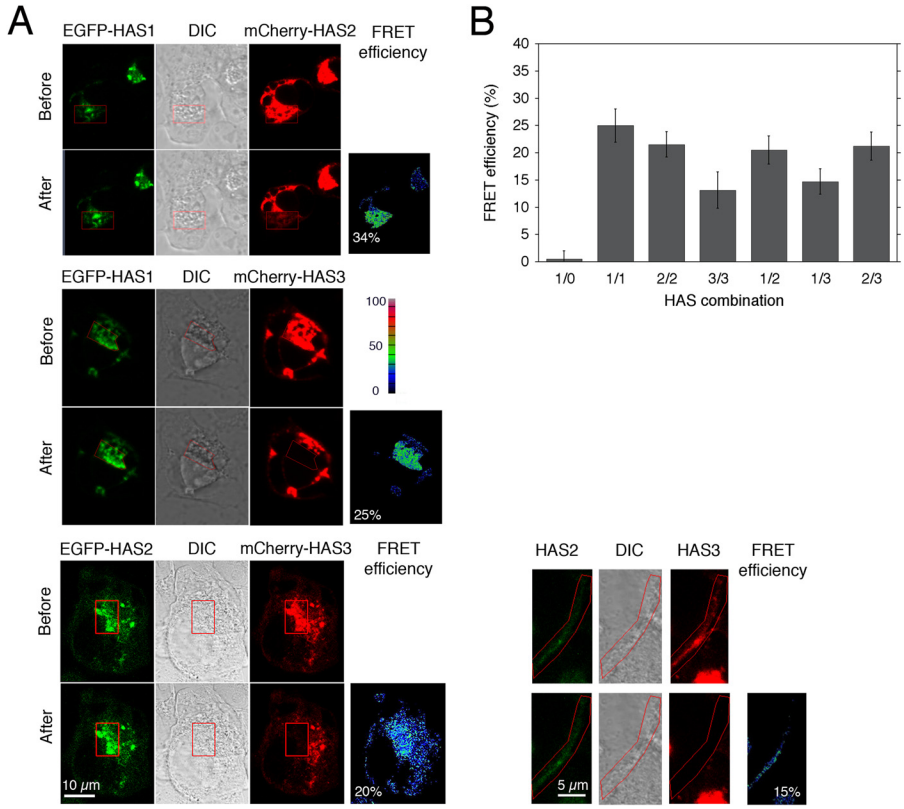

FIGURE 5. **FRET microscopy determined by donor fluorescence increase after acceptor photobleaching.** N-terminal EGFP- and mCherry-tagged HAS constructs were co-transfected in COS1 cells and imaged with confocal microscopy. *A*, examples of heteromeric interactions between HAS1/HAS2, HAS1/HAS3, and HAS2/HAS3. Emission of EGFP (*green*) before and after photobleaching of mCherry (*red*) is shown in photobleached regions of interest (marked by the *red line*). Differential interference contrast (*DIC*) images of the cells are shown between those of EGFP and mCherry. The *rightmost panels* show false color scaling of FRET efficiency. *B*, for each measurement, a FRET efficiency was calculated from the pre- and post-donor fluorescence intensities in the photobleached Golgi area as demonstrated by the *red* regions of interest in *A*. The average FRET efficiency of each HAS combination is expressed as the mean ± S.E. from 10–18 cells expressing both EGFP and mCherry. FRET efficiencies were calculated for all homo- and heteromeric HAS complexes (HAS1/1, HAS2/2, HAS3/3, HAS1/2, HAS1/3, and HAS2/3). EGFP-HAS1 with an empty mCherry vector is indicated by HAS1/0 and was used as a negative control. The FRET efficiencies of all HAS pairs were found to be significantly different from the FRET efficiency calculated for the negative control (HAS1/0) ($p < 0.05$, one-way analysis of variance with Dunnett's post hoc test).

HAS3. The numbers of dots detected with these antibody sets clearly exceeded the background level obtained by counting together the signals (dots) of each antibody alone. Preimmune rabbit sera when combined with the specific goat anti-HAS2 antibody also gave a background signal comparable to that of the antibody alone. These data indicate that endogenously expressed HAS proteins form homomeric and heteromeric complexes, thus excluding the possibility that the complexes arise only when HASs are over-expressed.

Domains of the HAS Polypeptides Involved in the Interactions—The FRET observed between the N-terminally tagged HAS constructs indicate that the distance between the N termini of two HAS proteins is less than 10 nm. Likewise, positive FRET in the C-terminally tagged HASs used for flow cytometry indicate that the C termini of the HAS complex partners were within 10 nm of each other. Interestingly, FRET was not observed when HAS3, labeled with mCherry in its C terminus, was co-transfected with EGFP in the N terminus of HAS1, HAS2, and HAS3 (data not shown). The absence of FRET suggests that the HAS complexes are organized in a manner such that the N and C termini of the two interacting HASs are beyond 10 nm of each other.

To find out which HAS domains are responsible for the interaction, microscopic FRET was performed with C-terminally truncated HAS1 containing EGFP in the N terminus. HAS1 missing all of the C-terminal transmembrane domains and part of the cytosolic putative glycosyltransferase domain (truncated at amino acid 143) still interacted with the full-length HAS2 that contained mCherry in its N terminus (Fig. 7*A*). Likewise, the N-terminal domain of HAS3, truncated at amino acid 166, produced a FRET signal with full-length HAS3 and HAS2, and also with HAS3 truncated at amino acid 220 (Fig. 7*A*). In contrast, HAS1 truncated close to the N terminus (amino acid 12) was not able to associate with HAS2 (Fig. 7*A*). These data suggest that a domain for HAS homo- and heteromeric formation is located close to the N-terminal part of the enzymes.

The presence of an interacting domain in the N-terminal part of HASs was confirmed by co-immunoprecipitation of full-length mCherry-HAS2 with EGFP-HAS3 C-terminally truncated at amino acid 86 (Fig. 7*B*). EGFP alone was not precipitated with mCherry-HAS2, indicating specific binding between the HASs (Fig. 7*B*). The HAS3 construct in which the N terminus was truncated at amino acid 86 and replaced by EGFP was also precipitated with HAS2. The latter finding indicates that there are other (or another) binding domains between the HAS polypeptides that reside outside of the N-terminal region. Western blots from cells transfected with intact and truncated GFP-HAS3 constructs also showed unidentified smaller bands,

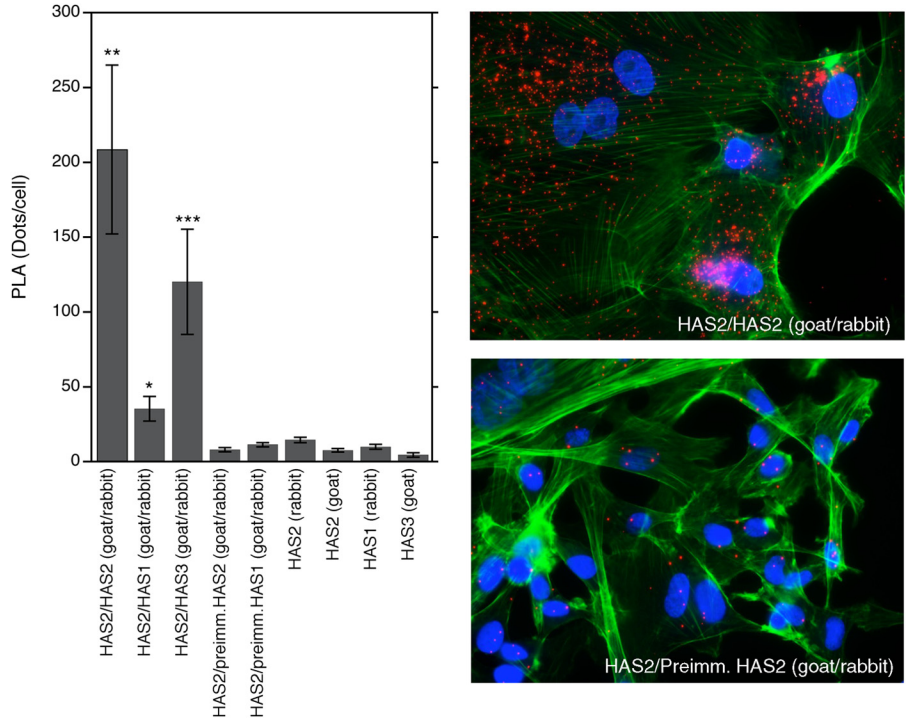

FIGURE 6. **Interactions detected by PLA among endogenous HAS1, HAS2, and HAS3 in mesothelial cells.** Pairs of goat and rabbit antibodies against HAS proteins, detected by DNA-labeled secondary antibodies, were ligated together when the proteins were close enough to interact and amplified into a fluorescent dot. The number of dots obtained by replacing the rabbit HAS1 and HAS2 antibodies with their respective preimmune sera or by omitting one of the antibodies represents the background signal. The micrographs show an example of the HAS2/HAS2 signal and its control with preimmune serum. The columns show the means ± S.E. of 5–11 images from two experiments. ***, $p < 0.0005$; **, $p < 0.005$; and *, $p < 0.01$; compared with the corresponding pair with preimmune serum (Wilcoxon-Mann-Whitney rank sum test).

partly enriched in and partly excluded from the immunoprecipitates (Fig. 7*B*). As shown above with HAS1 (Fig. 1), these may represent HAS3 that have lost fragments from the C terminus.

Hyaluronan Synthesis by the Enzyme Complexes—To evaluate whether the various HAS enzyme complexes are active and functionally relevant, we measured the ability of the three HASs, transfected alone and in different combinations, to synthesize and secrete hyaluronan into the extracellular medium.

Fig. 8*A* shows the normalized relative synthetic activities in the experimental set-up in which flow cytometry was used to measure the fluorescence of mCer and mVen, as described above. Although the synthesis was normalized to fluorescence (the level of HAS protein), the findings were similar without normalization (data not shown). The activity of HAS1 alone was found to be lowest and was therefore used as a reference value. In the COS7 cells used in these experiments, HAS2 and HAS3 had a 40- and 80-fold, respectively, higher activity than HAS1. Intriguingly, the highest activity was detected with the HAS2-HAS3 combination, ~2 times higher than the sum of the two transfected alone. In contrast, the HAS1-HAS3 combination did not significantly increase hyaluronan synthesis relative to HAS3 alone, whereas HAS1 and HAS2 co-expression showed markedly lower synthesis than HAS2 alone.

Hyaluronan synthesis by the different HAS combinations was also studied on a C8161 melanoma cell line in which we introduced stable expression of doxycycline-inducible EYFP-HAS2. The induced expression of EYFP-HAS2 was studied with and without transient HAS1-mVen and HAS3-mCer transfections. The induction-controlled expression of HAS2 reduced the variation in hyaluronan synthesis and increased the precision of the assays. These results confirmed the finding that introduction of HAS1 suppressed hyaluronan synthesis by HAS2, but its influence on hyaluronan synthesis by HAS3 was also inhibitory (Fig. 8*B*). In these cells and with this experimental set-up, hyaluronan synthesis by the HAS2-HAS3 combination was not additive but showed values close to HAS3 alone. Nevertheless, the data suggest that the different HAS isoforms have the potential to modulate hyaluronan synthesis by the other isoforms, suggesting cooperative functioning in hyaluronan synthesis through heteromerization.

DISCUSSION

The present work shows, for the first time, *in situ* complexes between HAS polypeptides in several cell types. These findings are in line with a previous report showing homomeric interactions between HAS2 and heteromeric interactions between HAS2 and HAS3 *in vitro* (33). The present data also indicate that all three HAS isoenzymes can form homo- and heteromeric complexes in live cells. Moreover, the PLA data show that this is also the case for endogenous HAS enzymes, thereby excluding the possibility that complex formation is merely the result of enzyme overexpression in the cells. These findings open completely novel vistas on the structure-function relationship of HASs.

These data are interesting in the light of a recent report on Golgi-localized glycosyltransferases involved in the processing of *N*- and *O*-linked oligosaccharides. These glycosyltrans-

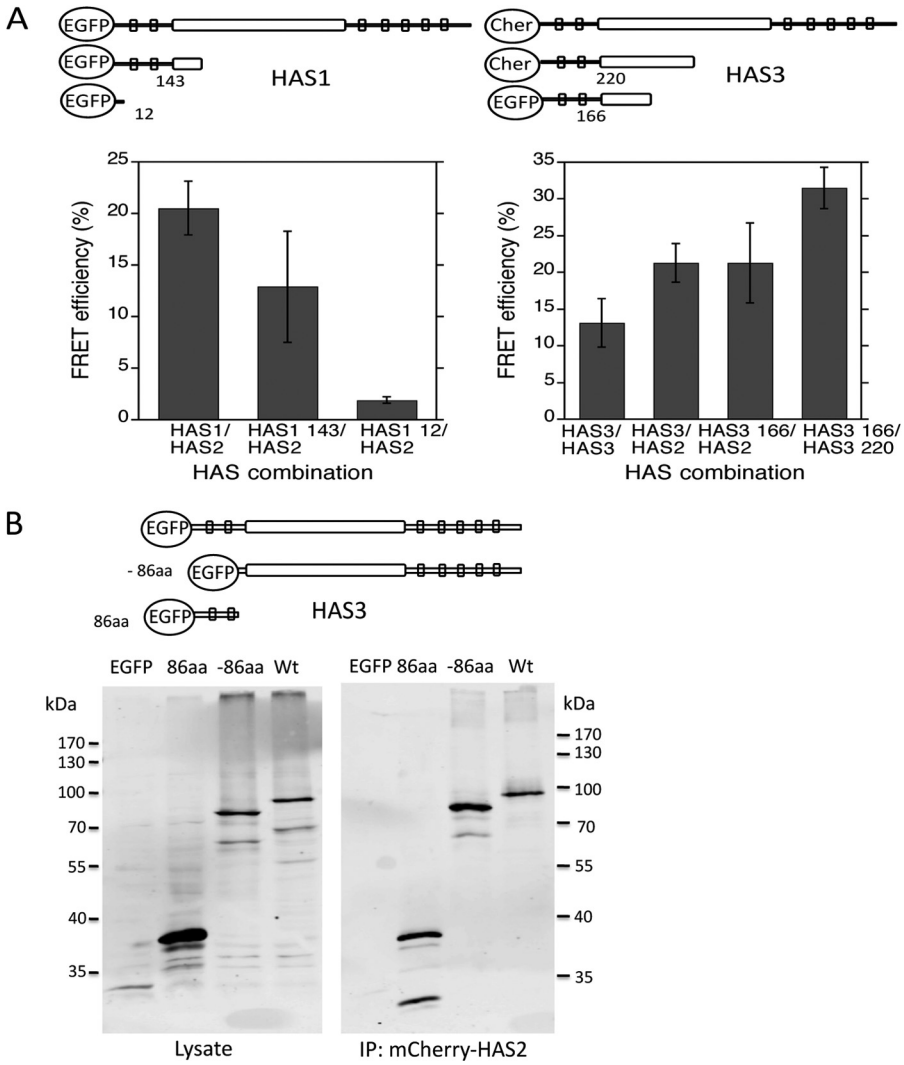

FIGURE 7. **Homomeric and heteromeric interactions with truncated HAS constructs.** *A*, the full-length and C-terminally truncated HAS1 and HAS3 constructs subjected to microscopic FRET are schematically illustrated at the *top*. The *larger horizontal boxes* represent the putative cytosolic glycosyltransferase domains, and the *small boxes* indicate the predicted transmembrane or membrane-associated domains. The transfected HAS combinations are indicated under the columns, and the truncated ones are marked by the *number* of their amino acids. Means ± S.E. of 7–15 determinations are shown. The difference in the FRET efficiency of HAS3/HAS3 *versus* HAS3–166 amino acids/HAS3–220 amino acids was statistically significant ($p < 0.05$, analysis of variance with Dunnett's post hoc test) *B*, full-length HAS3 and its N- and C-terminally truncated constructs, schematically illustrated at the *top*, were co-transfected with mCherry-HAS2. The complexes were precipitated with RFP-Trap M for red fluorescent proteins and analyzed by SDS-PAGE under reducing conditions followed by Western blotting using a GFP antibody to show the co-precipitated HAS3 constructs. Total cell lysates and the immunoprecipitates (*IP*) are shown in the *left* and *right blots*, respectively. The empty EGFP vector (*left lanes*) was used as a control (present in the lysate but not in the immunoprecipitate). The predicted molecular masses of intact EGFP-HAS3, −86aa EGFP-HAS3, 86aa EGFP-HAS3, and EGFP are 90, 80, 37, and 27 kDa, respectively.

ferases have also been shown to form both homomeric and heteromeric complexes *in situ* (35). In this particular case, heteromerization was found to take place only between sequentially acting enzymes. HAS enzymes, despite being active only at the plasma membrane, share the same tendency to form homo- and heteromers. Recent studies also have demonstrated homo- and heteromeric complexes between cell wall-synthesizing enzymes, *i.e.* chitin, cellulose, and poly-β-1,6-*N*-acetylglucosamine synthases (29, 31, 32). These enzymes resemble HASs in that they are also thought to form a pore in plasma membrane for extrusion of the growing polysaccharide chain. Altogether, our findings emphasize that complex formation might be a general property of perhaps all glycosyltransferases and that they function as larger units rather than as enzyme monomers as thought previously. Whether the complexes represent dimeric, tetrameric, or even higher oligomeric structures remains unclear at the moment. However, there are some indications that tetramers and even higher oligomers are involved. For example, digitonin-solubilized HAS1 fractionated on a gel filtration column shows enzymatically active HAS1 at a very high molecular mass (~600 kDa) (45). A part of the solubilized seHAS also elutes in a position corresponding to a dimer (17). The Golgi-localized GalT1 and ST6Gal1 transferase activities and proteins elute at the size of enzyme tetramers (34), but large oligomers have also been reported (46). Further structural studies will be necessary to resolve the exact composition of the HAS homomers and heteromers.

The C-terminal truncation experiments indicated that one of the sites mediating homo- and heteromeric binding was located between their N termini and the glycosyltransferase domains of

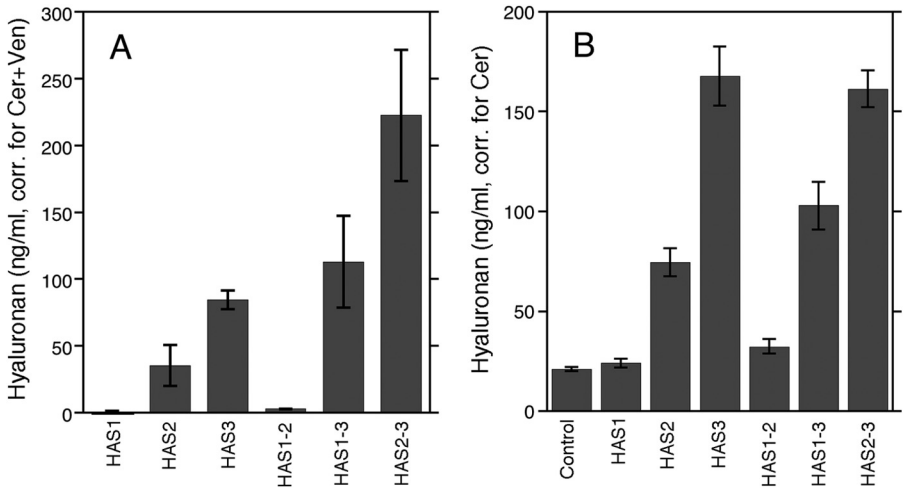

FIGURE 8. **Hyaluronan synthesis by the different HAS complexes.** *A*, HAS-mCer and HAS-mVen were transfected to COS7 cells and cultivated for 24 h after which the media were collected for the determination of hyaluronan levels. The cells were detached and analyzed for fluorescence by flow cytometry to allow calculation of the normalized relative activities of the various HAS complexes, as described under "Experimental Procedures." Each column represents the corrected values (mean + S.D.) from triplicate samples. HAS1 activity = 1 was used as a reference value. *B*, C8161 cells were stably transduced with the EYFP-HAS2 gene, the expression of which could be induced by doxycyclin. The cells were transiently transfected with mCer or mVen, with or without EYFP-HAS2 induction, using 0.25 μg/ml doxycyclin. The hyaluronan values were normalized to the mCer fluorescence of the cultures. The EYFP, mCer, and mVen fluorescence ratios in each of the pairs ranged between 0.70 and 1.15, suggesting roughly equal expressions of the constructs. The means ± S.E. of three separate experiments are shown. The decrease in the hyaluronan synthesis of HAS2 and HAS3 by co-transfection of HAS1 was statistically significant: $p < 0.05$ and $p < 0.001$, respectively, using repeated measures analysis of variance with Bonferroni corrections.

the interacting HAS proteins. However, truncation of this N-terminal part still allowed binding, indicating that additional binding sites exist also outside of this domain, closer to the C termini. More information about the interacting domains came from the FRET signals, which were positive between the N or C termini but negative between the N and C termini of the binding partners. This suggests that the interaction precludes the close proximity of the C and N termini of the interacting proteins.

The observed homo- and heteromerization among the different HAS isoenzymes introduces a number of important questions concerning their formation, trafficking, and physiological relevance in hyaluronan synthesis. For example, we showed that all of the complexes had strong FRET signals in the perinuclear Golgi region and less strong at the cell surface. This may be due to the predominant localization of the HAS polypeptides in the Golgi region and the relatively weaker signal at the plasma membrane. The data suggest that complex formation does not take place upon enzyme activation and the initiation of hyaluronan synthesis, which presumably occur at the plasma membrane, but rather has already occurred in the ER or the Golgi. Complex formation may, however, be a prerequisite for activation at the cell surface by other factors, or it may be necessary for HAS trafficking to the plasma membrane (21).

It is possible that the complexes are dynamic and freely interchangeable with each other. This would provide a rapid means of modulating either the activity or the trafficking of the complexes in response to physiological demands, which would be analogous to the formation of Golgi glycosyltransferase heteromers, in contrast to homomers, upon lowering the pH of the Golgi lumen (34).

Complex formation also raises interesting possibilities concerning the function of the HAS isoenzymes in hyaluronan synthesis. First, earlier data (33) suggest that the complexes are required for HAS activity, as co-transfection of a mutated, nonfunctional HAS2 inhibits hyaluronan synthesis by an intact HAS2 in a dominant negative manner. We also showed that introduction of HAS1 reduced the synthesis of hyaluronan by HAS2 and HAS3, suggesting that HAS1 heteromers are less active than HAS2-HAS2 and HAS3-HAS3 homomers.

However, in the present experiments, coupling the levels of hyaluronan synthesis to distinct HAS complexes should be regarded only as suggestive, as it is based on the assumption that the ratios and levels of co-transfected and overexpressed HAS isoenzymes mimic those that exist between endogenous HAS proteins. This may not be the case in each physiological condition, or in every cell type *in vivo*, given the variable expressions of HAS in different cell types (20, 47). In addition, the normalization of the hyaluronan synthesis to the amount (fluorescence intensity) of HAS protein may not correlate with the amount of active protein, part of which may have undergone denaturation or fragmentation. Because truncated HASs are also able to form complexes, they could potentially influence the enzymatic activity of native HAS proteins, perhaps in a dominant negative manner (33). It is also obvious that at any time point only a relatively small part of the total cellular HAS resides in the plasma membrane, the site of HA synthesis.

The exact proportions of the HASs in complexes *versus* monomers are not known, although the robust FRET signals suggest that the homo- and heteromers are common, if not the dominant form. Therefore, factors other than complex formation could also contribute to the observed changes in hyaluronan synthesis by the different HAS isoforms. Obviously, analyses of the association/dissociation constants between HASs, and their consequences in hyaluronan synthesis rate, are needed.

The expression levels of the different HASs are known to be highly dynamic. A stimulus often increases the expression of

two (48) or all three of the HASs (47, 49). Induction of the HAS isoforms occurs at different time points following a stimulus, lasts for different periods of time, and is mediated by different signaling pathways (49). The sequential HAS inductions are expected to create temporal changes in the stoichiometry between the HAS proteins, which can influence the rate of hyaluronan synthesis, as suggested by the present data. However, potential functions affected by the cooperation between HASs, besides the synthesis rate, also include the molecular mass of the hyaluronan and the way it is organized on the cell surface (20, 50).

An interesting corollary to the homo- and heteromeric organization of the HASs is that this arrangement might allow the sequential addition of GlcNAc and GlcUA by separate HAS polypeptides complexed with each other. This would solve the dilemma of how a single, relatively small protein with two transferase activities, which binds tightly to hyaluronan, could allow hyaluronan extrusion through a pore made by the enzyme itself. It can be speculated that processive rachet-like shifting of the growing polymer between the UDP-GlcNAc and UDP-GlcUA binding sites (15) could involve sites on separate but interacting HAS polypeptides, resembling the model suggested recently for seHAS (17). A larger pore through complex formation can also be envisioned to better accommodate hyaluronan extrusion. These and other possibilities warrant further exploration of the HAS protein quaternary structures and their functional consequences.

Acknowledgment—We thank Riikka Kärnä for skillful technical assistance.

REFERENCES

1. Laurent, T. C., Laurent, U. B., and Fraser, J. R. (1996) The structure and function of hyaluronan: an overview. *Immunol. Cell Biol.* **74,** A1–A7
2. Tammi, M. I., Day, A. J., and Turley, E. A. (2002) Hyaluronan and homeostasis: a balancing act. *J. Biol. Chem.* **277,** 4581–4584
3. Bakkers, J., Kramer, C., Pothof, J., Quaedvlieg, N. E., Spaink, H. P., and Hammerschmidt, M. (2004) Has2 is required upstream of Rac1 to govern dorsal migration of lateral cells during zebrafish gastrulation. *Development* **131,** 525–537
4. Camenisch, T. D., Schroeder, J. A., Bradley, J., Klewer, S. E., and McDonald, J. A. (2002) Heart-valve mesenchyme formation is dependent on hyaluronan-augmented activation of ErbB2-ErbB3 receptors. *Nat. Med.* **8,** 850–855
5. Tolg, C., Hamilton, S. R., Zalinska, E., McCulloch, L., Amin, R., Akentieva, N., Winnik, F., Savani, R., Bagli, D. J., Luyt, L. G., Cowman, M. K., McCarthy, J. B., and Turley, E. A. (2012) A RHAMM mimetic peptide blocks hyaluronan signaling and reduces inflammation and fibrogenesis in excisional skin wounds. *Am. J. Pathol.* **181,** 1250–1270
6. Thorne, R. F., Legg, J. W., and Isacke, C. M. (2004) The role of the CD44 transmembrane and cytoplasmic domains in co-ordinating adhesive and signalling events. *J. Cell Sci.* **117,** 373–380
7. Kozlova, I., Ruusala, A., Voytyuk, O., Skandalis, S. S., and Heldin, P. (2012) IQGAP1 regulates hyaluronan-mediated fibroblast motility and proliferation. *Cell. Signal.* **24,** 1856–1862
8. Misra, S., Toole, B. P., and Ghatak, S. (2006) Hyaluronan constitutively regulates activation of multiple receptor tyrosine kinases in epithelial and carcinoma cells. *J. Biol. Chem.* **281,** 34936–34941
9. Li, L., Asteriou, T., Bernert, B., Heldin, C. H., and Heldin, P. (2007) Growth factor regulation of hyaluronan synthesis and degradation in human dermal fibroblasts: importance of hyaluronan for the mitogenic response of PDGF-BB. *Biochem. J.* **404,** 327–336
10. Porsch, H., Bernert, B., Mehić, M., Theocharis, A. D., Heldin, C. H., and Heldin, P. (2013) Efficient TGFβ-induced epithelial-mesenchymal transition depends on hyaluronan synthase HAS2. *Oncogene* **32,** 4355–4365
11. Provenzano, P. P., Cuevas, C., Chang, A. E., Goel, V. K., Von Hoff, D. D., and Hingorani, S. R. (2012) Enzymatic targeting of the stroma ablates physical barriers to treatment of pancreatic ductal adenocarcinoma. *Cancer Cell* **21,** 418–429
12. McDonald, T. O., Gerrity, R. G., Jen, C., Chen, H. J., Wark, K., Wight, T. N., Chait, A., and O'Brien, K. D. (2007) Diabetes and arterial extracellular matrix changes in a porcine model of atherosclerosis. *J. Histochem. Cytochem.* **55,** 1149–1157
13. Kang, L., Lantier, L., Kennedy, A., Bonner, J. S., Mayes, W. H., Bracy, D. P., Bookbinder, L. H., Hasty, A. H., Thompson, C. B., and Wasserman, D. H. (2013) Hyaluronan accumulates with high-fat feeding and contributes to insulin resistance. *Diabetes* **62,** 1888–1896
14. Oikari, S., Jokela, T., Tammi, R., and Tammi, M. (2012) Multiple roles of hyaluronan as a target and modifier of the inflammatory response, in *Extracellular Matrix: Pathobiology and Siganaling* (Karamanos, N., ed) pp. 39–65, Walter De Gruyter & Co., Berlin
15. Weigel, P. H., and DeAngelis, P. L. (2007) Hyaluronan synthases: a decade-plus of novel glycosyltransferases. *J. Biol. Chem.* **282,** 36777–36781
16. Tammi, R. H., Passi, A. G., Rilla, K., Karousou, E., Vigetti, D., Makkonen, K., and Tammi, M. I. (2011) Transcriptional and post-translational regulation of hyaluronan synthesis. *FEBS J.* **278,** 1419–1428
17. Hubbard, C., McNamara, J. T., Azumaya, C., Patel, M. S., and Zimmer, J. (2012) The hyaluronan synthase catalyzes the synthesis and membrane translocation of hyaluronan. *J. Mol. Biol.* **418,** 21–31
18. Prehm, P. (1984) Hyaluronate is synthesized at plasma membranes. *Biochem. J.* **220,** 597–600
19. Rilla, K., Siiskonen, H., Spicer, A. P., Hyttinen, J. M., Tammi, M. I., and Tammi, R. H. (2005) Plasma membrane residence of hyaluronan synthase is coupled to its enzymatic activity. *J. Biol. Chem.* **280,** 31890–31897
20. Rilla, K., Oikari, S., Jokela, T. A., Hyttinen, J. M., Kärnä, R., Tammi, R. H., and Tammi, M. I. (2013) Hyaluronan synthase 1 (HAS1) requires higher cellular UDP-GlcNAc concentration than HAS2 and HAS3. *J. Biol. Chem.* **288,** 5973–5983
21. Deen, A. J., Rilla, K., Oikari, S., Kärnä, R., Bart, G., Häyrinen, J., Bathina, A. R., Ropponen, A., Makkonen, K., Tammi, R. H., and Tammi, M. I. (2014) Rab10-mediated endocytosis of the hyaluronan synthase HAS3 regulates hyaluronan synthesis and cell adhesion to collagen. *J. Biol. Chem.* **289,** 8375–8389
22. Medina, A. P., Lin, J., and Weigel, P. H. (2012) Hyaluronan synthase mediates dye translocation across liposomal membranes. *BMC Biochem.* **13,** 2
23. Hagenfeld, D., Borkenhagen, B., Schulz, T., Schillers, H., Schumacher, U., and Prehm, P. (2012) Hyaluronan export through plasma membranes depends on concurrent K+ efflux by K(ir) channels. *PLoS One* **7,** e39096
24. Thomas, N. K., and Brown, T. J. (2010) ABC transporters do not contribute to extracellular translocation of hyaluronan in human breast cancer in vitro. *Exp. Cell Res.* **316,** 1241–1253
25. Siiskonen, H., Rilla, K., Kärnä, R., Bart, G., Jing, W., Haller, M. F., DeAngelis, P. L., Tammi, R. H., and Tammi, M. I. (2013) Hyaluronan in cytosol-microinjection-based probing of its existence and suggested functions. *Glycobiology* **23,** 222–231
26. Tlapak-Simmons, V. L., Kempner, E. S., Baggenstoss, B. A., and Weigel, P. H. (1998) The active streptococcal hyaluronan synthases (HASs) contain a single HAS monomer and multiple cardiolipin molecules. *J. Biol. Chem.* **273,** 26100–26109
27. Pummill, P. E., Kempner, E. S., and DeAngelis, P. L. (2001) Functional molecular mass of a vertebrate hyaluronan synthase as determined by radiation inactivation analysis. *J. Biol. Chem.* **276,** 39832–39835
28. Bobrov, A. G., Kirillina, O., Forman, S., Mack, D., and Perry, R. D. (2008) Insights into *Yersinia pestis* biofilm development: topology and co-interaction of Hms inner membrane proteins involved in exopolysaccharide production. *Environ. Microbiol.* **10,** 1419–1432
29. Steiner, S., Lori, C., Boehm, A., and Jenal, U. (2013) Allosteric activation of exopolysaccharide synthesis through cyclic di-GMP-stimulated protein-protein interaction. *EMBO J.* **32,** 354–368

30. Smirnova, I., Kasho, V., and Kaback, H. R. (2011) Lactose permease and the alternating access mechanism. *Biochemistry* **50,** 9684–9693
31. Morgan, J. L., Strumillo, J., and Zimmer, J. (2013) Crystallographic snapshot of cellulose synthesis and membrane translocation. *Nature* **493,** 181–186
32. Merzendorfer, H. (2006) Insect chitin synthases: a review. *J. Comp. Physiol. B* **176,** 1–15
33. Karousou, E., Kamiryo, M., Skandalis, S. S., Ruusala, A., Asteriou, T., Passi, A., Yamashita, H., Hellman, U., Heldin, C. H., and Heldin, P. (2010) The activity of hyaluronan synthase 2 is regulated by dimerization and ubiquitination. *J. Biol. Chem.* **285,** 23647–23654
34. Hassinen, A., Pujol, F. M., Kokkonen, N., Pieters, C., Kihlström, M., Korhonen, K., and Kellokumpu, S. (2011) Functional organization of Golgi *N*- and *O*-glycosylation pathways involves pH-dependent complex formation that is impaired in cancer cells. *J. Biol. Chem.* **286,** 38329–38340
35. Hassinen, A., Rivinoja, A., Kauppila, A., and Kellokumpu, S. (2010) Golgi *N*-glycosyltransferases form both homo- and heterodimeric enzyme complexes in live cells. *J. Biol. Chem.* **285,** 17771–17777
36. Kokkonen, N., Rivinoja, A., Kauppila, A., Suokas, M., Kellokumpu, I., and Kellokumpu, S. (2004) Defective acidification of intracellular organelles results in aberrant secretion of cathepsin D in cancer cells. *J. Biol. Chem.* **279,** 39982–39988
37. Bastiaens, P. I., Majoul, I. V., Verveer, P. J., Söling, H. D., and Jovin, T. M. (1996) Imaging the intracellular trafficking and state of the AB5 quaternary structure of cholera toxin. *EMBO J.* **15,** 4246–4253
38. Rilla, K., Pasonen-Seppänen, S., Deen, A. J., Koistinen, V. V., Wojciechowski, S., Oikari, S., Kärnä, R., Bart, G., Törrönen, K., Tammi, R. H., and Tammi, M. I. (2013) Hyaluronan production enhances shedding of plasma membrane-derived microvesicles. *Exp. Cell Res.* **319,** 2006–2018
39. Shin, K. J., Wall, E. A., Zavzavadjian, J. R., Santat, L. A., Liu, J., Hwang, J. I., Rebres, R., Roach, T., Seaman, W., Simon, M. I., and Fraser, I. D. (2006) A single lentiviral vector platform for microRNA-based conditional RNA interference and coordinated transgene expression. *Proc. Natl. Acad. Sci. U.S.A.* **103,** 13759–13764
40. Tammi, R., Ågren, U. M., Tuhkanen, A. L., and Tammi, M. (1994) Hyaluronan metabolism in skin. *Prog. Histochem. Cytochem.* **29,** 1–81
41. Hiltunen, E. L., Anttila, M., Kultti, A., Ropponen, K., Penttinen, J., Yliskoski, M., Kuronen, A. T., Juhola, M., Tammi, R., Tammi, M., and Kosma, V. M. (2002) Elevated hyaluronan concentration without hyaluronidase activation in malignant epithelial ovarian tumors. *Cancer Res.* **62,** 6410–6413
42. Kultti, A., Rilla, K., Tiihonen, R., Spicer, A. P., Tammi, R. H., and Tammi, M. I. (2006) Hyaluronan synthesis induces microvillus-like cell surface protrusions. *J. Biol. Chem.* **281,** 15821–15828
43. Müllegger, J., Rustom, A., Kreil, G., Gerdes, H. H., and Lepperdinger, G. (2003) "Piggy-back" transport of *Xenopus* hyaluronan synthase (XHAS1) via the secretory pathway to the plasma membrane. *Biol. Chem.* **384,** 175–182
44. Törrönen, K., Nikunen, K., Kärnä, R., Tammi, M., Tammi, R., and Rilla, K. (2014) Tissue distribution and subcellular localization of hyaluronan synthase isoenzymes. *Histochem. Cell Biol.* **141,** 17–31
45. Asplund, T., Brinck, J., Suzuki, M., Briskin, M. J., and Heldin, P. (1998) Characterization of hyaluronan synthase from a human glioma cell line. *Biochim. Biophys. Acta* **1380,** 377–388
46. Opat, A. S., Houghton, F., and Gleeson, P. A. (2000) Medial Golgi but not late Golgi glycosyltransferases exist as high molecular weight complexes: role of luminal domain in complex formation and localization. *J. Biol. Chem.* **275,** 11836–11845
47. Yamada, Y., Itano, N., Hata, K., Ueda, M., and Kimata, K. (2004) Differential regulation by IL-1β and EGF of expression of three different hyaluronan synthases in oral mucosal epithelial cells and fibroblasts and dermal fibroblasts: quantitative analysis using real-time RT-PCR. *J. Invest. Dermatol.* **122,** 631–639
48. Declèves, A. E., Caron, N., Voisin, V., Legrand, A., Bouby, N., Kultti, A., Tammi, M. I., and Flamion, B. (2012) Synthesis and fragmentation of hyaluronan in renal ischaemia. *Nephrol. Dial. Transplant.* **27,** 3771–3781
49. Rauhala, L., Hämäläinen, L., Salonen, P., Bart, G., Tammi, M., Pasonen-Seppänen, S., and Tammi, R. (2013) Low dose ultraviolet B irradiation increases hyaluronan synthesis in epidermal keratinocytes via sequential induction of hyaluronan synthases Has1–3 mediated by p38 and Ca2+/calmodulin-dependent protein kinase II (CaMKII) signaling. *J. Biol. Chem.* **288,** 17999–18012
50. Siiskonen, H., Kärnä, R., Hyttinen, J. M., Tammi, R. H., Tammi, M. I., and Rilla, K. (2014) Hyaluronan synthase 1 (HAS1) produces a cytokine- and glucose-inducible, CD44-dependent cell surface coat. *Exp. Cell Res.* **320,** 153–163